Structure and Characterization of Nanocomposite Langmuir−Blodgett Films of Poly(maleic monoester)/Fe_3O_4 Nanoparticle Complexes

Don Keun Lee and Young Soo Kang*

Department of Chemistry, Pukyong National University, 599-1 Daeyeon-3-dong, Nam-gu, Pusan 608-737, Korea

Choong Sub Lee

Department of Physics, Pukyong National University, 599-1 Daeyeon-3-dong, Nam-gu, Pusan 608-737, Korea

Pieter Stroeve

Department of Chemical Engineering and Material Science, University of California, Davis, California 95616

Received: December 10, 2001; In Final Form: April 30, 2002

Nanocomposite Langmuir−Blodgett films of poly(maleic monoester) (PMA)/Fe_3O_4 nanoparticles were prepared by transferring PMA/iron oxide nanoparticles complex monolayers in a hydrosol subphase of Fe_3O_4 nanoparticles onto solid substrates. A Mössbauer spectrum of the nanoparticles showed the highly crystalline nature of the magnetite structure. Homogeneous dispersion of Fe_3O_4 nanoparticles between poly(maleic monoester) layers was observed with transmission electron microscopy (TEM), and surface morphology of the nanocomposite film was studied with atomic force microscopy (AFM). The magnetic properties of the Fe_3O_4 nanoparticles and the nanocomposite Langmuir−Blodgett film of poly(maleic monoester) (PMA)/Fe_3O_4 nanoparticles were studied with vibrating magnetometry (VSM) by obtaining magnetic hysteresis loops. The PMA is a polymeric surfactant and interacts with Fe_3O_4 nanoparticles by electrostatic attraction between carboxylate groups of PMA and the charged Fe_3O_4 nanoparticles. This interaction stabilizes the homogeneous dispersion of nanoparticles between the PMA polymer layers. The surface morphology, as shown by AFM images, gives well-formed surface structures that were evenly spaced by iron oxide nanoparticles. The average height of one layer of the PMA/iron oxide nanocomposite film is determined to be 12.9 nm and this is approximately consistent with the summation of the PMA thickness and the average iron oxide diameter with an average roughness of 3.3 nm. The cross sectional AFM image also shows homogeneous distinct single domains of Fe_3O_4 nanoparticles in the nanocomposite film.

Introduction

The preparations and properties of nanoparticles of metals, semiconductors, and insulators have been studied and reported in the literature.[1−3] An important task is to assemble these nanoparticles in an ordered structure and maintain their isolated particle properties.[4,5] Nanocomposites composed of organic/inorganic hybrid films of nanoparticles are under intensive current research. Materials with particle diameters in the range of 1 to 10 nm exhibit novel electronic, optical, magnetic, and chemical properties due to their extremely small dimensions.[6] Although several studies have been devoted to the synthesis of nanometer-sized compound semiconductors, relatively little work exists for magnetic materials of similar dimensions.[7−10] Potential applications for the latter exist in information storage,[11,12] color imaging,[10] bioprocessing,[13,14] magnetic refrigeration,[14] and ferro-fluids.[15] Such materials may also serve as models for small magnetic particles, which may comprise a portion of interstellar dust.[16]

A critical obstacle in assembling and maintaining nanoscale materials from nanoparticle clusters is the tendency of the latter to aggregate in order to reduce the energy associated with a high ratio of surface area to volume. By using surfactants, attempts have been made to stabilize, isolate, and prepare homogeneously dispersed metal oxide micro-size particles into organic materials.[17] An interesting method for preparing ultrathin metal oxide films has been mentioned elsewhere.[18,19] The preparation and characterization of magnetic Fe_3O_4 nanoparticle/nanocomposite monolayers at the air/water interface has been reported in our laboratories.[20,21,23−25,27] Ordered complexes of magnetic organic surfactant/ nanoparticle can be prepared by the Langmuir−Blodgett (L-B) technique and the degree of nanoparticle dispersion can be observed with TEM. The surface morphology and surface distribution of nanoparticles in the films can be studied with atomic force microscopy.

In the present study, magnetic Fe_3O_4 nanoparticles were synthesized in aqueous solution and the Langmuir behavior of Fe_3O_4 poly(maleic monoester)/nanoparticle complexes at the air/water interface were studied with surface pressure−area isotherms. The nanocomposite multilayer films of Fe_3O_4 poly(maleic monoester)/nanoparticle were prepared by depositing the poly(maleic monoester) (PMA) monolayer on the subphase of an Fe_3O_4 nanoparticle hydrosol. The dispersion of iron oxide nanoparticles in the PMA Langmuir−Blodgett film was observed with TEM by depositing the Langmuir monolayer on the surface of copper grids. The magnetic properties of Fe_3O_4 nanoparticles and the multilayered L-B films of Fe_3O_4 poly(maleic monoester)/nanoparticle were studied with vibrating

10.1021/jp014446t CCC: $22.00
Published on Web 06/27/2002

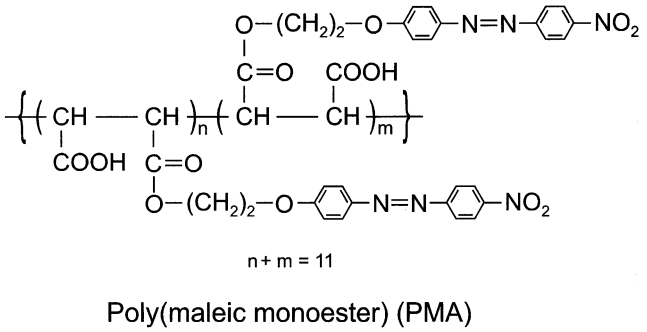

Figure 1. The structure of poly(maleic monoester) (PMA).

sample magnetometry (VSM). The surface morphology, the degree of dispersion of Fe_3O_4 nanoparticles in the poly(maleic monoester), and the film thickness of a layer of the nanocomposite film were characterized with AFM.

Experimental Section

The chemicals $FeCl_2$ (anhydrous, 99+%) and $FeCl_3$ (anhydrous, 99+%) were obtained from Aldrich Chemical Co. and used without any further purification. The nanoparticles of Fe_3O_4 were synthesized by the procedure described before.[20,21] The average diameter of the Fe_3O_4 nanoparticles was 8.8 ± 0.8 nm as determined with TEM (JEOL 200CX). Mössbauer spectra were recorded using a conventional Mössbauer spectrometer of the electromechanical type with a 20 mCi ^{57}Co source in an Rh matrix. To produce a uniform thickness over the area of the Mössbauer absorber, each sample was mixed with boron nitride powder. The area density of Fe for the flattened sample was 10 mg/cm^2. The PMA structure is shown in Figure 1. The PMA was synthesized by the procedure described previously.[22] Measurement of the pressure−area isotherms and L-B film preparation was performed with a KSV MINITROUGH. The clear hydrosol of Fe_3O_4 nanoparticles in water was prepared at pH = 4.0 and used as the subphase of Langmuir layers. The concentration of iron ion in the hydrosol was determined as 9.29×10^{-5} M with an atomic absorption spectrophotometer (Shimadzu AA-680). The pressure−area isotherms of PMA in pure water and hydrosol of iron oxide were obtained at room temperature. The L-B films of the PMA/ Fe_3O_4 nanoparticle complex were prepared by transferring the Langmuir layer at a surface pressure of 25 mN/m. The TEM images were obtained with a JEOL 200CX. The magnetization curves and hysteresis loops of the nanocomposite films were characterized with a Lake Shore 7300 VSM. Atomic force microscopy images were obtained with an AUTOPROBES CP from Digital Instruments with AFM contact mode; 1.6 mm × 1.6 mm scan size and 3 Hz scan rate. The average thickness of the PMA/Fe_3O_4 nanoparticle complex film was obtained using software from Digital Instruments.

Results and Discussion

The synthesized Fe_3O_4 nanoparticles, with an average diameter less than 10 nm, were completely oxidized into γ-Fe_2O_3 in a time period of about two weeks. This conversion was measured by FT-IR, colorimetric titration, and Mössbauer spectroscopy.[23,24,27] Mössbauer spectrum of the synthesized nanoparticles is shown in Figure 2. The spectrum was deconvoluted to two sextets that correspond to iron ions in tetrahedral (T_d) A and octahedral (O_h) B sites of magnetite. Fe_3O_4 can be written as $Fe^{3+}(Fe^{2+}\ Fe^{3+})O_4$. A fast electron-transfer process (electron hopping) between Fe^{2+} and Fe^{3+} ions on the O_h B site takes place above 110−120 K. The spectrum shows clearly two hyperfine magnetic splitting, which are a clear evidence for magnetite. The nanoparticles that we synthesized can be definitely defined as Fe_3O_4, but a few of the particles can be in the γ-Fe_2O_3 form due to the time from synthesis to use in the PMA/ Fe_3O_4 complex studies (approximately 3 days). Thus, nanoparticles in the present study are clearly defined as Fe_3O_4.

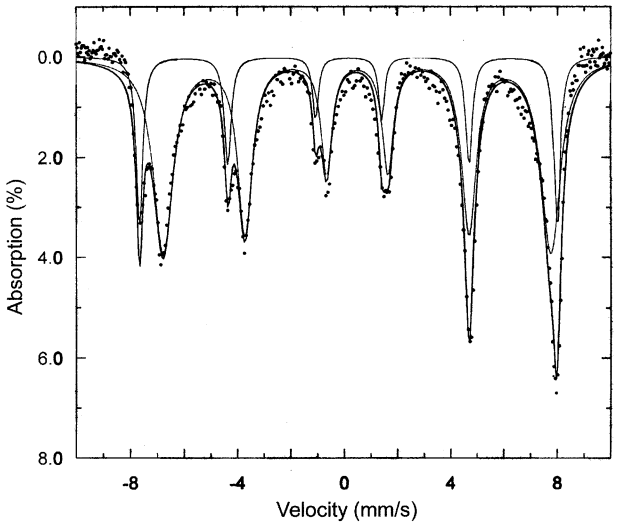

Figure 2. Computer-fitted Mössbauer spectrum of Fe_3O_4 nanoparticles at room temperature.

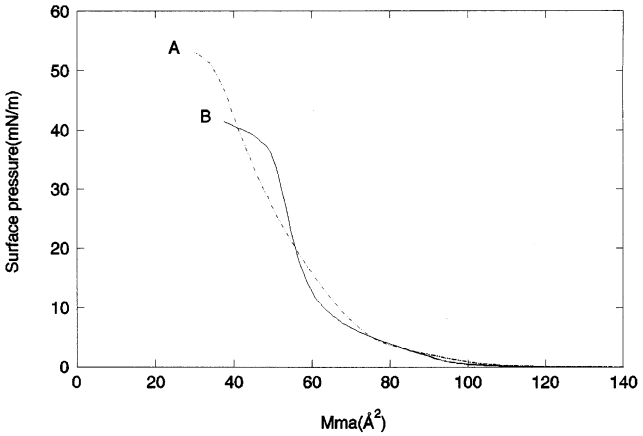

Figure 3. Surface pressure−area isotherms of poly(maleic monoester) in subphase of pure water (A) and Fe_3O_4 nanoparticle hydrosol (B).

The pressure−area isotherms of PMA monolayers at the air/water interface in pure water and Fe_3O_4 nanoparticle hydrosol subphase are shown in Figure 3. The isotherms of the PMA monolayer in the pure water, compared to the Fe_3O_4 nanoparticle hydrosol subphase, showed a similar mean molecular area at surface pressures up to 20 mN/m. Above 20 mN/m the mean molecular area is somewhat expanded. These results are in contrast to previous studies with the surfactants poly(octadecene-*co*-maleic anhydride), stearic acid, and arachidic acid where the isotherms on iron oxide nanoparticle hydrosol subphases were significantly expanded in comparison to a pure water subphases at all surface pressures.[21,24,25] The previous results were explained by complexation of the iron oxide nanoparticles with the carboxylate groups of the surfactant monolayers. Complexation was caused by electrostatic interactions between the positive surface charge of the iron oxide nanoparticle and the negatively charged carboxylate groups of the surfactants. The ionic bonding by electrostatic interactions between iron oxide nanoparticles and carboxylate groups has been identified by FT-

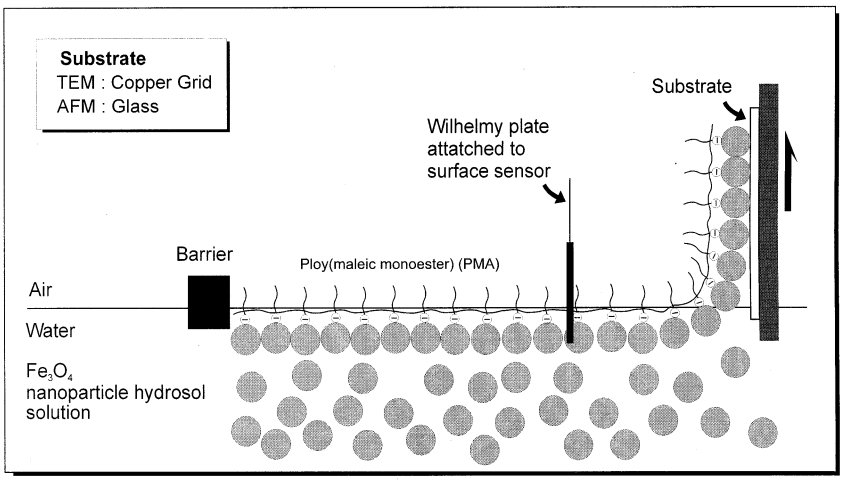

Figure 4. Schematic drawing of Langmuir−Blodgett deposition of poly(maleic monoester)/Fe_3O_4 nanoparticles complex monolayer at the air/water interface.

IR studies.[24] The degree of isotherm expansion of the monolayer at the air/water interface is critically dependent on the distance between carboxylate groups of the polymer backbone on the monolayer. The expansions of the isotherms of poly(octadecene-*co*-maleic anhydride), stearic acid , and arachidic acid monolayers at the air/water interface are caused by the short distances between carboxylate groups in the monolayers compared with the size of the iron oxide nanoparticles. The carboxylate groups can be expanded from each other by the interactions with the iron oxide nanoparticles with diameters much larger than the distance between carboxylate groups. This effect is not dominant in the PMA monolayer in the present study because the distances between carboxylate groups are large enough so that they are not significantly expanded by interactions with the iron oxide nanoparticles.

The interaction of carboxylate groups in the monolayer with Fe_3O_4 nanoparticles is schematically shown in Figure 4. The lower collapse point of the monolayer on pure water subphase compared to the Fe_3O_4 nanoparticle hydrosol subphase, as shown in Figure 3, can be explained by the distorted structure of the monolayer at the air/water interface. The distorted structure is presumably caused by the bulky nanoparticle complexation with the monolayer. The L-B film of the PMA/Fe_3O_4 nanoparticles complex was prepared by transferring the monolayer at the air/water interface onto a solid substrate as shown in Figure 4. The deposition was carried out at a surface pressure of 25 mN/m at room temperature and gave a Y-type Langmuir−Blodgett film. Higher surface pressures resulted in the crystallization of the Langmuir monolayer at the air/water interface. This was also reported in the previous studies.[21] Further, low surface pressures resulted in an inhomogeneous dispersion of the Fe_3O_4 nanoparticles in the L-B film.

The dispersion of Fe_3O_4 nanoparticle in the L-B film of PMA was studied by TEM and a typical image is shown in Figure 5. The TEM image from the L-B deposition of two layers onto the copper grid shows a homogeneous dispersion of Fe_3O_4 nanoparticles. The electrostatic interactions between carboxylate groups of PMA and Fe_3O_4 nanoparticles prevent aggregation of clumps of the nanoparticles on the monolayer. Our previous study also reported on homogeneous dispersion of iron oxide nanoparticles with other surfactant molecules.[26] The homogeneously dispersed Fe_3O_4 nanoparticles result in a single layer of nanoparticles between layers of PMA in L-B deposition. The stacking of iron oxide nanoparticles between the PMA layers by increasing the number of deposited layers was previously

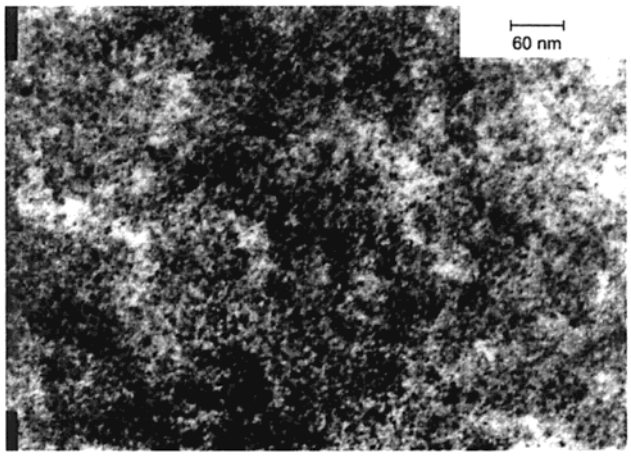

Figure 5. A TEM image of a 2-layers Langmuir−Blodgett film of poly(maleic monoester)/Fe_3O_4 nanoparticles deposited onto copper grid. The TEM image was taken with a 100 000 magnification.

investigated and showed increasing optical absorbance of iron oxide nanoparticles in nanocomposite films.[24]

The magnetic properties of Fe_3O_4 nanoparticles and Langmuir-Blodgett films of Fe_3O_4 nanoparticle/PMA complex were studied with VSM at room temperature and at 20 K. Bulk Fe_3O_4 is ferromagnetic at room temperature, but below a critical particle size Fe_3O_4 becomes superparamagnetic and shows no remanence or coercivity. The magnetic properties of γ-Fe_2O_3 nanoparticles and γ-Fe_2O_3 stearic acid/nanoparticle complexes were studied with VSM in a previous report.[23] Figure 6A,B,C,D show magnetization curves as a function of applied magnetic field for both Fe_3O_4 nanoparticles (A and B) and for Langmuir−Blodgett films of PMA/Fe_3O_4 nanoparticles complex (C and D) at room temperature and at 20 K. No hysteresis at room temperature indicates superparamagnetic behavior (Figure 6A,C). Below the blocking temperature, magnetic nanoclusters become magnetically frozen. The magnetic moment of the nanoclusters is fixed, and the remanence and coercivity in the hysteresis loop appear on the plot of magnetization as a function of magnetic field.[28−30] Magnetization plots at 20 K are shown in Figure 6B for the Fe_3O_4 nanoparticles. A smaller hysteresis loop, which is symmetric about the center, is apparent for the L-B film (Figure 6D). The nanoparticles and the complex L-B film show similar behavior at room temperature and at 20 K.

The image and surface morphology of L-B films of PMA/iron oxide nanoparticles were characterized with AFM. The

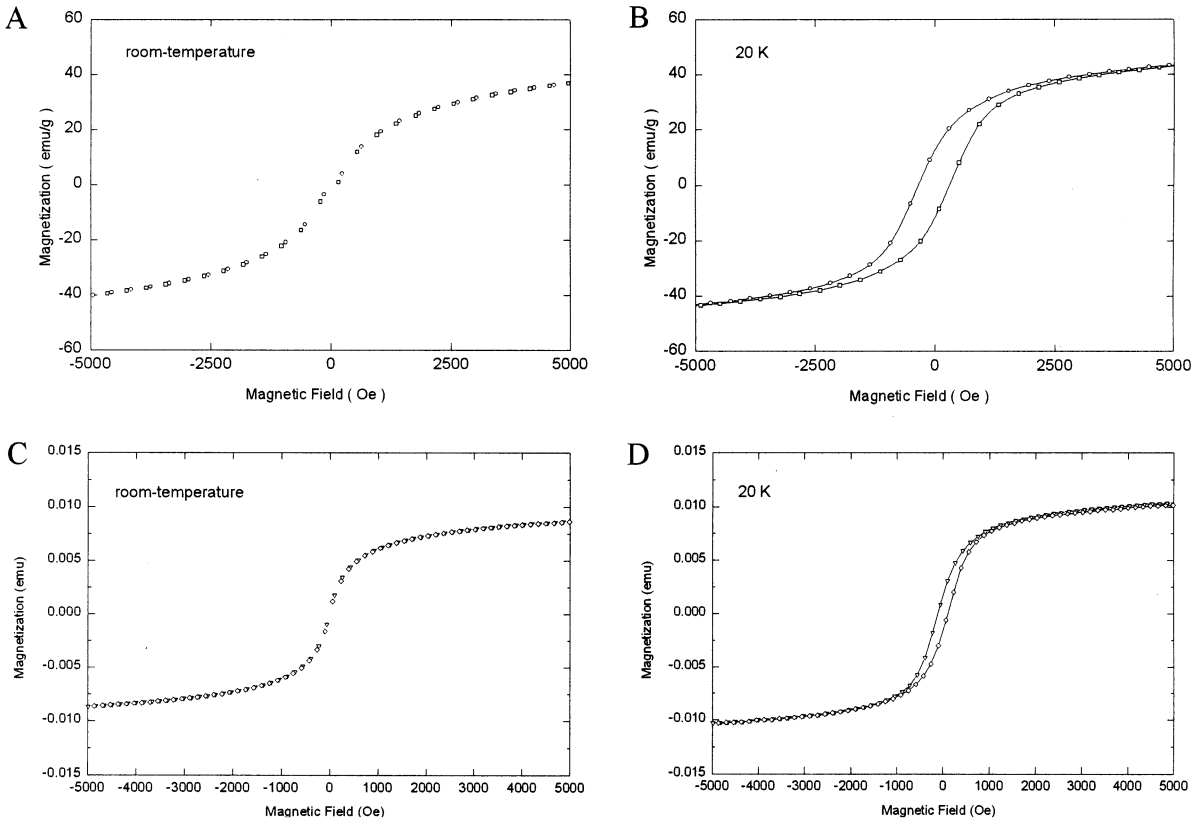

Figure 6. Magnetic hysteresis loop of Fe_3O_4 nanoparticles at room temperature (A), and 20 K (B); and of a 100-layers Langmuir−Blodgett film of poly(maleic monoester)/Fe_3O_4 nanoparticles complex at room temperature (C), and 20 K (D) obtained from a vibrating sample magnetometer (VSM).

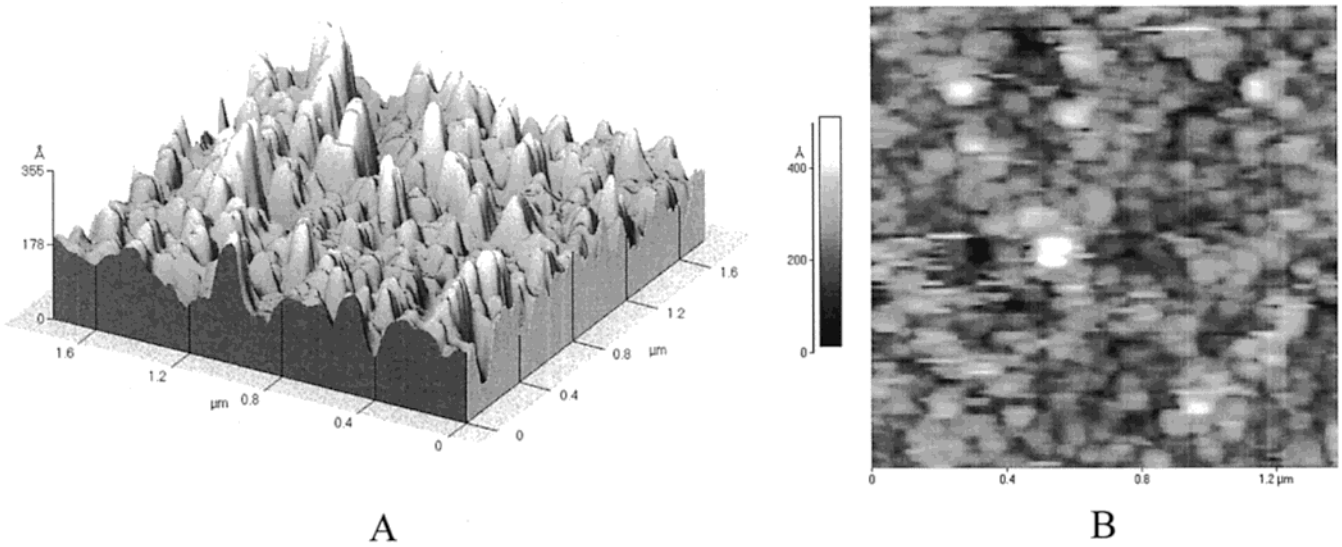

Figure 7. Three-dimensional surface structure morphology (A), and cross-sectional surface image (B) of a one-layer Langmuir−Blodgett film of poly(maleic monoester)/Fe_3O_4 nanoparticle complex deposited onto a glass surface as obtained by atomic force microscopy.

surface morphology of bare glass used as a solid substrate for the film deposition was scanned for comparison before deposition. The surface morphology and cross sectional image of a one-layer L-B film of PMA/iron oxide nanoparticles are shown in Figure 7. The morphology shows peaks caused by the iron oxide nanoparticles coated with the PMA film. The average peak height of the L-B film corresponds to the sum of the PMA thickness and the average iron oxide particle diameter and is 12.9 nm with an average roughness of 3.3 nm. This indicates that the one-layer L-B film of PMA/iron oxide nanoparticles was homogeneously deposited on the glass surface. This is consistent with a L-B transfer ratio of 1. This supposition was furthermore verified with the average peak height of a two-layer L-B film that had an average peak height of 25.6 nm and an average roughness of 4.2 nm. The cross-sectional image of a one-layer L-B film shows a distinct single domain of the iron oxide nanoparticle (Figure 7).

A schematic interlayer structure of the deposited Y-type L-B film is shown in Figure 8. The iron oxide particles are deposited between PMA layers by electrostatic interactions between the positive surface charge of the iron oxide nanoparticles and the negative charge of the carboxylate groups of PMA.

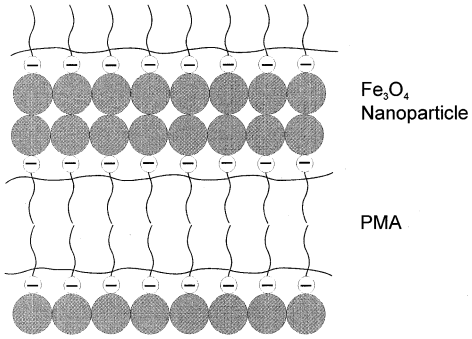

Figure 8. Schematic drawing of Y-type Langmuir−Blodgett films of poly(maleic monoester)/Fe_3O_4 nanoparticle composite.

In conclusion, the dispersion of iron oxide nanoparticles between polymer layers is homogeneous as determined by TEM and shown in Figure 5. The iron oxide particles covered with PMA have organized surface morphology. The L-B film of iron oxide particles covered with PMA show well-formed surface morphology by showing peaks representing the iron oxide nanoparticles. The cross-sectional image of a one-layer L-B film showed distinct domains of the iron oxide nanoparticles. The magnetic properties of the L-B films were studied with VSM. The hysteresis loops of magnetization as a function of applied magnetic field showed superparamagnicity at room temperature and a small coercivity at 20 K.

Acknowledgment. This research was supported by Korea Research Foundation Grant (KRF-2001-015-DP0365).

References and Notes

(1) Brus, L. E. *J. Phys. Chem.* **1986**, *90*, 2555.
(2) Fendler, J. H. *Chem. Rev.* **1987**, *87*, 877.
(3) Henglein, A. *Chem. Rev.* **1989**, *89*, 1861.
(4) Stucky, G. D.; MacDougall, J. E. *Science* **1990**, *247*, 669.
(5) Brus, L. E. *J. Mater. Res.* **1989**, *4*, 704.
(6) Mann, S.; Hannington, J. P. *J. Colloid Interface Sci.* **1988**, *122*, 326.
(7) Zhao, X. K.; Herve, P. J.; Fendler, J. H. *J. Phys. Chem.* **1989**, *93*, 908.
(8) Papaefthymiou, V. *J. Appl. Phys.* **1990**, *67*, 4487.
(9) Shull, R. D. *J. Appl. Phys.* **1990**, *67*, 4490.
(10) Ziolo, R. F. U.S. Patent 4,474,866, 1984.
(11) Gunther, L. *Phys. World* **1990**, *3*, 28.
(12) Audran, R. G. L.; Huguenard, A. P. U.S. Patent 4,302,523, 1981.
(13) Nixon, L.; Koval, C. A.; Noble, R. D.; Slaff, G. S. *Chem. Mater.* **1992**, *4*, 117.
(14) Marchessault, R. H.; Richard, S.; Rioux, P. *Carbohydrate Res.* **1992**, *224*, 133.
(15) McMichael, R. D.; Shull, R. D.; Schuwartzendruber, L. J.; Bennett, L. H.; Watson, R. E. *J. Magn. Magn. Mater.* **1992**, *111*, 29.
(16) Anton, I. *J. Magn. Magn. Mater.* **1990**, *85*, 219.
(17) Huffman, D. R. *Adv. Phys.* **1977**, *26*, 219.
(18) Shah, D. M.; Chan, W. K.; Bhat, R.; Cox, H. M.; Schlotter, N. E.; Chang, C. C. *Appl. Phys. Lett.* **1990**, *56*, 2132.
(19) Chan, W. K.; Chang, G. K.; Bhat, R.; Schlotter, N. E.; Nguyen, C. K. *IEEE Electron Device Lett.* **1989**, *10*, 417.
(20) Kang, Y. S.; Risbud, S.; Rabolt, J. F.; Stroeve, P. *Chem. Mater.* **1996**, *8*, 2209.
(21) Kang, Y. S.; Risbud, S.; Rabolt, J. F.; Stroeve, P. *Langmuir* **1996**, *12*, 4345.
(22) Peng, X. G.; Gao, M. L.; Zhao, Y. Y.; Kang, S. H.; Zhang, Y. H.; Zhang, Y.; Wang, D. J.; Xiao, L. Z.; Li, T. J. *Chem. Phys. Lett.* **1993**, *209*, 233.
(23) Lee, D. K.; Moon, S. D.; Kang, Y. S.; Lee, C. S. *Korea Polym. J.* **1998**, *6*, 367.
(24) Kang, Y. S.; Lee, D. K.; Stroeve, P. *Thin Solid Films* **1998**, *327*, 541.
(25) Lee, D. K.; Kang, Y. S. *Mol. Cryst. Liq. Cryst.* **1998**, *316*, 153.
(26) Porter, M. R. *Recent Developments in the Technology of Surfactants*; Elsevier: Orlando, FL, 1990.
(27) Kang, H. J.; Lee, C. S.; Kim, D.; Kang, Y. S.; Kim, Y. I. *Bull. Korean Chem. Soc.* **1998**, *19*, 408.
(28) Sohn, B. H.; Cohen, R. E. *Chem. Mater.* **1997**, *9*, 264.
(29) Vassiliou, J. K.; Mehrotra, V.; Russell, M. W.; Giannelis, E. P.; McMicjael, R. D.; Shull, R. D.; Ziolo, R. F. *J. Appl. Phys.* **1993**, *73*, 5109.
(30) Cullity, B. D. *Introduction to Magnetic Materials*; Addision-Wiley: Reading, MA, 1972.